Energy materials

Dopamine as a bioinspired adhesion promoter for the metallization of multi-responsive phase change microcapsules

Cordelia Zimmerer[1],*, Giulia Fredi[2],*, Sascha Putzke[1], Regine Boldt[1], Andreas Janke[1],
Beate Krause[1], Astrid Drechsler[1], and Frank Simon[1]

[1] *Leibniz-Institut Für Polymerforschung Dresden E.V, Hohe Str. 6, 01069 Dresden, Germany*
[2] *Department of Industrial Engineering and INSTM Research Unit, University of Trento, Via Sommarive 9, 38123 Trento, Italy*

ABSTRACT

This work reports on an environmentally friendly method to produce encapsulated phase change material with a thin nickel coating, applicable for heat conversion, storage and thermal management of heat-sensitive components and suitable for active heating by electromagnetic radiation. A critical issue for the metallization is the adhesion between the polymer capsule shell and the metal layer. Based on previous studies using the bio-molecule dopamine as adhesion promoter in composites and for plastics metallization, commercial paraffin microcapsules were coated with an ultrathin polydopamine film via a simple wet chemical process. Subsequently, a thin, uniform and compact nickel layer was produced by electroless metallization. The successful deposition of both layers was verified with a broad range of imaging and spectroscopic techniques. For the first time, surface-enhanced IR spectroscopy was used to study the deposition of ultrathin PDA films. The combination of SEM and energy-dispersive X-ray spectroscopy allowed resolving the spatial distribution of the elements Ni, N, and O in the MC shell. Electrically conducting paths in the Ni shell were verified by conductive AFM. Thermal analysis revealed that the coated microcapsules show a phase change enthalpy of approx. 170 J/g, suitable for thermal storage and management. Additionally, the nickel layer enhanced the thermal diffusivity of the microcapsule powders and enables a fast heating of the PCM microcapsules by microwave radiation, demonstrating the applicability of the metallized MCs for controlled heating applications.

GRAPHICAL ABSTRACT
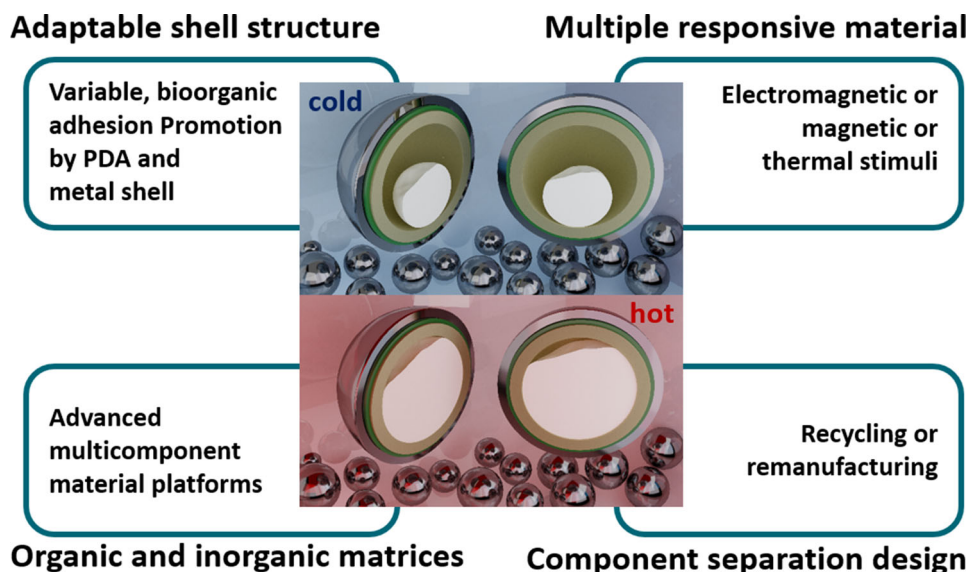
Introduction

Organic solid–liquid phase change materials (PCM) are of high relevance for manifold applications requiring thermal management or storage [1]. These materials, generally paraffin waxes, fatty acids, or poly(ethylene glycol)s, absorb thermal energy by melting and stabilize the temperature to a value near their melting point. Upon cooling and solidification, they release the latent heat. For most applications, PCMs have to be encapsulated in macro-, micro-, or nano-shells to avoid leakage, loss of material, contamination or reactions with the environment [2, 3]. The shell consists of inorganic, polymer or hybrid materials [3], provides mechanical stability [4] and increases the specific surface area of the PCM, thereby promoting the heat exchange despite the typically low thermal conductivity of organic PCMs [5]. Encapsulated PCMs are easier to handle and can be embedded in bulk materials, fibers, or thin films to provide thermoregulating properties [6–11]. Such composite materials have a high potential for applications, e.g., in construction materials [12], packaging [13], anti-icing coatings [14], or solar energy collectors [5]. In the field of electronics, PCM capsules can be

incorporated into substrates, housings, sealings, and cases, to provide thermal stabilization of miniature electronic devices [15].

Important parameters for the performance of PCM capsules are their energy storage capacity, thermal conductivity, chemical, thermal and mechanical stability and fire resistance [16]. A promising way to enhance the thermal conductivity is the application of a metallic shell or coating on the capsule surface [3]. As additional benefit, metallization allows preparation of capsules with tailored electrical and magnetic properties. This widens the field of their applications significantly. Metallized PCM capsules can be heated actively by radiation-induced stimulation of the metal shell while the temperature is stabilized by the PCM inside the capsules. Energy can be transferred by electromagnetic irradiation, magnetic or inductive or electrical stimulation. Moreover, the metal surface makes the capsules compatible to other metals allowing the preparation of electrically and thermally conductive composites with a continuous metal phase applicable for thermal stabilizing of electrically conducting elements, as microwave absorbers for internal retard heating elements, or as magnetic field barrier. The higher thermal conductivity of the metal matrix is

expected to provide a better cooling effect than polymer composites. Furthermore, metal-compatible organic filler particles might be of interest for mechanical enhancement in lightweight applications or scratch-resistant surfaces with a metallic optical apparition.

From the literature, several examples are known for the in situ metal encapsulation of oily droplets in emulsions [17–19]. The application of a metal film on capsules with a polymeric shell is much more challenging due to the incompatibility of most polymers with metals. The metallization of macroscopic polymer surfaces usually requires energy-intensive etching and activation steps using hazardous substances, is restricted to few selected polymers [20] and therefore not applicable to PCM microcapsules. In the literature, several attempts are described for depositing silver on microparticles or –capsules. To bind the silver on melamine–formaldehyde PCM capsules, Cao et al. [21] activated them with tin chloride. Wang [22] was the first to use the bio-based adhesion promoter dopamine (DA) as chelating agent for the deposition of silver on polystyrene microparticles. A similar approach was used by Zhu [23] to produce a silver layer on silica-coated PCM microcapsules. Al-Shannaq et al. produced silver layers on home-made PMMA-encapsulated PCM [24] and commercial capsules with a melamine resin shell [25]. This coating added about 25% to the capsule mass. It improved their thermal conductivity but reduced the latent heat. In all these studies, an array of silver clusters was formed instead of a continuous metal layer.

Previous studies of the authors [26, 27] used of DA to promote the adhesion of PCM microcapsules in polymeric composites. It had been shown that surface modification with DA-based layers greatly enhances their adhesion to an epoxy matrix, resulting in an increased thermomechanical performance of the composites, even at higher PCM content (up to 40 wt%). The reasons behind the excellent adhesion performance of DA and PDA are to be sought after in their unique chemistry. The catecholamine neurotransmitter DA is a small-molecule mimic of L-DOPA, the adhesive component of adhesive mussel proteins [28, 29]. Although its exact chemical composition and reaction mechanisms are still under debate [30], it is known that it contains various functional groups like Brønsted acidic catechol and basic amino groups that enable it to bind to a great

variety of surfaces. In alkaline aqueous environments, DA forms polymer-like films on solid surfaces. To simplify the scenario, the deposited film is named polydopamine (PDA) but its chemical structure is far from that of regular and well-defined traditional polymers. It can be finely tuned by varying the substrate, process technology, deposition parameters, and pre- or post-treatments [28, 31–33]. Adhesion and cohesion are based on covalent and non-covalent coupling and complex binding abilities. Adhesion is further supported by a molecular shrinkage during polymer formation, which results in a mechanical crumpling or gripping due to the intrinsic substrate surface roughness. By varying the deposition parameters, the coating thickness can be adjusted between a few and several hundreds of nanometers; a higher thickness is usually accompanied by a higher roughness.

The manifold binding abilities, reaction pathways and resulting structures of PDA allow universal adhesion on organic, inorganic and even on very-low
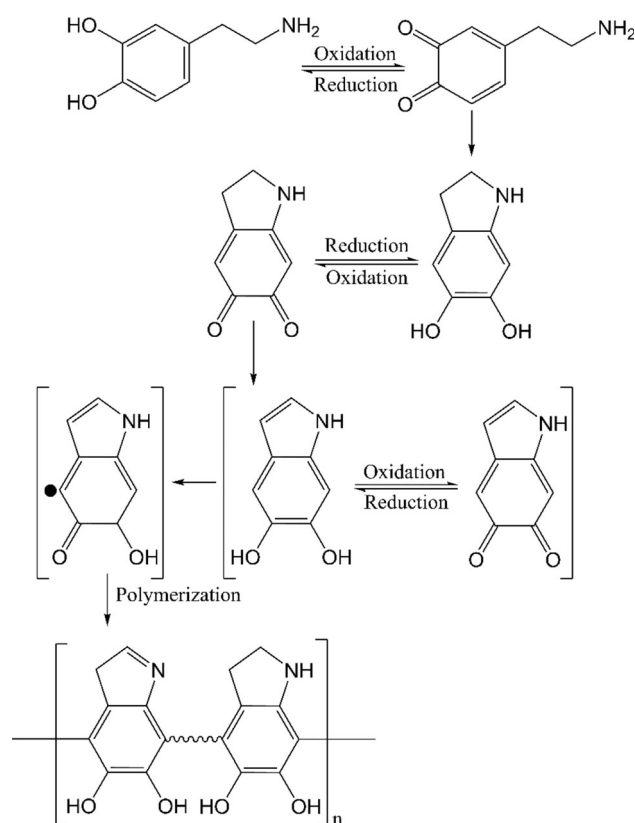

Figure 1 Simplified reaction scheme for dopamine deposition including a variety of chemical transformations, oligomerization, polymerization, and assembling of the variety of formed molecular structures.

surface free energy materials [28, 31, 32]. Under slightly alkaline conditions, DA can undergo different oxidation reactions, cyclization, condensations, rearrangements and covalent coupling reactions leading to oligomers and polymer structures, see Fig. 1 [30]. These complex sequences of organic reactions provide a universal, eco-friendly coating technology and a powerful platform for composite design. The DA deposition technology by adopted immersion coating and the substrate-supported polymerization of DA to PDA are simple and need neither time- and energy-consuming process steps nor hazardous chemicals [34–36]. This surface coating can be applied on microparticles and fibers as well as on larger and flat or curved surfaces [26, 27, 37, 38].

Thus, the easy and environmentally friendly deposition of PDA has a high potential to substitute energy-intensive processes and the use of hazardous substances, e.g., in the metallization of plastics [39, 40]. With regard to sustainability, PDA as adhesion promoter offers the additional benefit of being biodegradable [28] which allows a separation of composites at the end of their lifetime and re-use or recycling of the components [34].

In recent studies, we have shown that PDA modification enables electroless metallization of polymer surfaces with nickel [35, 36, 41]. The best results were obtained with an ultrathin PDA film deposited for only 10 min. The present study combines these findings with those about the PDA modification of PCM microcapsules [24–27] and proposes a method to coat commercial paraffin microcapsules with an ultrathin PDA film, followed by electroless metallization with nickel. In contrary to previous studies [23–25], this work employs a much shorter PDA deposition time and the less expensive nickel instead of the noble metal silver, which makes the process and the product less expensive. Moreover, the thinner metal layer created in this work allows retaining most of the pristine heat storage/release performance of the uncoated microcapsules, unlike previous studies that report a considerable reduction in the overall latent heat. In addition to an enhanced thermal and electrical conductivity, this treatment aims at introducing a response to electromagnetic stimuli.

The microcapsules were characterized thoroughly with regard to surface morphology, shell thickness and structure, chemistry, electrical properties,

thermal properties and degradation. A special challenge is the verification of the PDA deposition by surface-sensitive spectroscopy techniques [42]. For the first time, surface-enhanced IR spectroscopy is used for this purpose. A proof of concept is given for the microwave-stimulated MC heating. It is found that the ideal coating is thin (little mass and volume added, not to decrease too much the core-to-shell mass ratio and the phase change enthalpy) and provides thermal and electrical powder conductivity.

In a forthcoming study, the metallized PCM microcapsules will be embedded in an epoxy matrix. The final aim is to produce mixed-material composites able to be heated via Joule's effect, store thermal energy through the core's melting transition, and release heat when the temperature drops below the crystallization temperature of the core. These composites are intended to be used for thermal management of cold-sensitive items, e.g., electronic devices.

Materials and methods

Chemicals

Paraffin microcapsules Microtek MPCM43D, from now on labeled MCs, were purchased from Microtek Laboratories (Dayton, OH, USA). They consist of a paraffin wax core with a melting temperature of 43 °C (PCM phase) and a formaldehyde-based resin shell. According to the manufacturer, their average diameter is 17–20 μm and their melting enthalpy is 190–200 J/g. Dopamine hydrochloride (99%, DA) was purchased from Thermo Fisher GmbH, Germany. For the TRIS buffer, 2-amino-2 (hydroxymethyl) propane-1,3-diol (> 99.9%, Sigma-Aldrich, St. Louis, MI, USA) was first dissolved in deionized water (0.055 μS/cm) and then adjusted to pH 8.5 with hydrochloric acid (37%, HCl, VWR International, France). Ammonium hydroxide (28–30 wt% solution of ammonia in water [NH$_3$·H$_2$O], Acros Organics B.V.B.A., Belgium) was used to adjust the pH of the metallization solutions. For the production of the metallization bath series, the baths UDIQUE® 879 W, UDIQUE® accelerator 8810, UDIQUE® 891 nickel and UDIQUE® 893 stabilizer from the company MacDermit Enthone GmbH (Germany) company were employed in accordance with their usage instructions.

Dopamine modification of microcapsules

0.1 g of the MCs were immersed for 10 min in a stirred bath (500 rpm) containing aqueous solutions of 2 g/L DA and 10 mM TRIS buffer at pH 8.5, adjusted with hydrochloric acid. After this modification step, the coated MCs were separated from the solution with a glass frit (porosity G3, DWK Life Sciences GmbH Germany), rinsed with deionized water and dried under vacuum at 25 °C.

Metallization of PDA-modified microcapsules

The PDA-coated MCs were electroless metallized with nickel in a bath series from MacDermit Enthone GmbH (Germany). First, the MCs were placed in a palladium activator bath (UDIQUE® 879 W) at 30 °C for 3 min and then washed in a glass frit (G3) with deionized water. In a second step, the MCs were activated in an activator bath (UDIQUE® accelerator 8810) for 2.5 min at 50 °C, then filtered and washed in a glass frit. Finally, the MCs were placed in a nickel electrolyte bath (UDIQUE® 891 nickel and UDIQUE® 893 stabilizer) and coated with nickel for 8 min at 30 °C at a pH value of approx. 9. Then, they were washed with deionized water and dried under vacuum in a drying oven at 25 °C.

Characterization of the microcapsules

Confocal microscopy Confocal microscopy intensity images were obtained using a Scandisc confocal microscope µSurf expert (Nanofocus AG, Oberhausen, Germany) with the 100 × objective and maximal illumination.

Scanning electron microscopy (SEM) images of the MCs were acquired using an ULTRA Plus (Carl Zeiss Jena GmbH, Oberkochen, Germany) scanning electron microscope (SEM) at 3 kV acceleration voltage and applying the SE2 detector. The capsules were sputtered with a 3 nm platinum film. Cross-cuts of the MCs were prepared to study the layer morphology and thickness. For this purpose, the MCs were embedded in epoxy resin EpoFix Kit (Struers Inc., Cleveland, USA); the surface was cut smooth with a diamond knife. The cross-cuts were sputtered with a thin film of carbon before examination. EDX images were taken with an EDX detector XFlash 5060F (Bruker, Germany) with an accelerating voltage of 6 keV. In order to characterize the chemical composition and the elemental distribution across the layer, both sum spectra and hypermaps were recorded at different magnifications.

Atomic Force Microscopy (AFM) measurements were done with a Dimension ICON AFM (Bruker-Nano, USA). For imaging, the capsules were attached to a glass slide by a thin film of instant adhesive LOCTITE® 454™ (Henkel AG & Co. KGaA, Düsseldorf, Germany). The images were taken on the highest point of each capsule in soft tapping mode using Multi75-Al cantilevers by Budget sensors (Bulgaria) with a free cantilever amplitude of 500 mV and damping of 85%. Images were analyzed using the software NanoScope Analysis 1.90 (Bruker-Nano, USA). To emphasize the surface morphology and calculate roughness values, selected images were second-order flattened to remove the spherical shape of the capsules.

Conductive atomic force microscopy (C-AFM) measurements were done in contact mode with a Dimension ICON AFM equipped with a Peak Force TUNA application module for measurement of the contact current, and Ir/Pt-coated silicon SPM sensors SCM-PIT-V2 (Bruker-Nano, USA) with a nominal spring constant of 3 N/m and a tip radius < 25 nm. To assure electrical contact with the conductive substrate, the capsules were contacted by silver paste. A voltage of 300 mV was applied during the scan; the chosen sensitivity was 1 nA/V.

X-ray photoelectron spectroscopy (XPS) was carried out by means of an Axis Ultra photoelectron spectrometer (Kratos Analytical, Manchester, UK) equipped with a monochromatic Al Kα (h·v = 1486.6 eV) X-ray source of 300 W at 15 kV. The kinetic energy of photoelectrons was determined with a hemispheric analyzer set to pass energy of 160 eV for wide-scan spectra and 20 eV for high-resolution spectra. For XPS analyses, the MCs were prepared as dense particle films onto a double-sided adhesive tape (Scotch, 3 M, Maplewood, MN, U.S) mounted on the spectrometer's sample holder. During all measurements, electrostatic charging of the sample was avoided by means of a low-energy electron source working in combination with a magnetic immersion lens. Later, all recorded peaks were shifted by the value necessary to set the C 1 s peak to 285.00 eV. Quantitative elemental compositions were determined from peak areas using experimentally determined sensitivity factors and the spectrometer transmission function.

Spectrum background was subtracted according to Shirley [43]. The high-resolution spectra were deconvoluted by means of the Kratos spectra deconvolution software. Free parameters of component peaks were their binding energy (BE), height, full width at half maximum and the Gaussian–Lorentzian ratio.

Fourier transform infrared spectroscopy (FTIR) spectra from samples and from reference compounds were recorded in ATR mode using a FTIR spectrometer Vertex 70v (Bruker Optik GmbH, Ettlingen, Germany) equipped with a horizontal ATR diamond crystal unit (Platinum ATR diamond unit, Bruker Optik GmbH, Ettlingen, Germany) under vacuum (< 1 hPa) with an DLa-TGS-Detektor. 100 scans were co-added, averaged and Fourier transformed. The spectral resolution was set to 2. Spectra were analyzed using the OPUS package 7.5 (Bruker Optik GmbH, Ettlingen, Germany) and Origin 2020 (OriginLab Corporation, Northampton, 020,063–2 Massachusetts, USA). For surface-enhanced IR absorption spectroscopy (SEIRA), silver clusters were grown on the MC surfaces by wet chemical metallization.

Differential scanning calorimetry (DSC): DSC analysis was performed on neat and coated MCs with a Mettler DSC 30 calorimeter (Mettler Toledo, Inc., Columbus, OH, USA), at 10 °C/min, in the temperature range − 0/80 °C under a nitrogen flow of 100 ml/min. Specimens of approx. 5 mg were sealed in aluminum crucibles and subjected to a heating–cooling-heating cycle. The test allowed the measurement of the melting and crystallization temperatures (T_m, T_c) and enthalpies (ΔH_m, ΔH_c) of the MCs. Two specimens were tested per sample, to verify the repeatability.

Thermogravimetric analysis (TGA): TGA was carried out with a Q5000IR thermobalance (TA Instruments, Inc., NewCastle, DE, USA). Specimens of approx. 5 mg were tested at 10 °C/min up to 700 °C, under a nitrogen flow of 10 ml/min. Since a precise onset temperature could not be identified, the beginning of the thermal degradation was detected by calculating the temperatures corresponding to a mass loss of 1 wt %, 3 wt %, and 5 wt% ($T_{1\%}$, $T_{3\%}$, $T_{5\%}$). Moreover, the test allowed the measurement of the degradation temperature (T_d), intended as the peak of the derivative thermogravimetry (DTG) signal and corresponding to the temperature at the maximum degradation kinetics, and the residual mass after the test (m_r). Two specimens were tested per sample, to verify the repeatability.

Thermal powder diffusivity: Light flash analysis (LFA) was performed to measure the thermal diffusivity of the MC powder beds. The thermal diffusivity was measured at 25 °C, 40 °C and 55 °C with a light flash apparatus LFA 467 Hyperflash (NETZSCH-Gerätebau GmbH, Selb, Germany) equipped with a pressure sample holder, suitable to test the thermal diffusivity of powder beds pressed between two aluminum layers under a controllable torque. Specimens were prepared by sieving the PCM powders with a 63-μm metallic sieve, filling the sample holder with approx. 20 mg of PCM powder, and applying a torque of 15 cN·m. One specimen was tested per composition, and five pulses were performed per specimen. Thermal diffusivity (α) was determined using the software Proteus® (NETZSCH) provided with the instrument, by applying the three-layer model with linear baseline and numerical pulse correction. The calculation of the diffusivity with this specific sample holder is possible only by providing the specific heat of the material (c_P) and the density of the prepared specimen (ρ). The c_P was determined with the aforementioned DSC equipment by following the standard ASTM E1269, by using weight-matched aluminum crucibles and sapphire as the reference material.

Electrical powder resistivity The electrical resistivity of MC powders was measured using the PuLeMe instrument (home-built by Leibniz-Institut für Polymerforschung Dresden e.V.) [44]. The powder was filled into a cylinder, and the resistance between two movable electrodes was measured depending on the pressure. The resistance was measured with the multimeter DMM2001 (Keithley Instruments, Cleveland, OH, USA) which can determine resistances up to 1 GΩ. The given values are averages of two measurements.

Microwave treatment was first performed on loose MC powder. Approximately 0.5 g of modified MCs were spread and placed on a glass dish. The entire sample was placed in a microwave oven MW 5000 (Landgraf Laborsystem HLL GmbH, Germany, radiation frequency: 2450 MHz, radiated power: 500 W). To measure the temperature, the samples were briefly removed from the microwave oven and directly examined with the thermal imaging camera, Voltcraft® WB-300 (Conrad Electronic SE, Germany). Additionally, a poly(lactic acid) (PLA) film with embedded MCs was prepared to visualize the effect of the microwave treatment. For this purpose, 0.9 g

PLA were dissolved in 20 ml chloroform (99% + , stabilized with ethanol, Acros Organics BVBA, Belgium). 10 ml of the PLA chloroform solution were poured into a Petri dish (diameter 5 cm) and allowed to dry for 4 h under vacuum (10 mbar) at 25 °C. Then, about 0.1 g of metallized MCs were cast on the partly dried PLA film, and the remaining PLA solution was poured over the MCs. Afterward, the PLA-MC film was fully dried for 4 h under vacuum (10 mbar) at 25 °C.

Results

Two-step modification of the microcapsules

The metallization of the microcapsules combines two approaches applied successfully in former work of our group: the modification of MCs with DA to improve their adhesion in polymer-based composites [26, 27] and the use of DA as an adhesion promoter in the metallization of flat polymer surfaces [41]. In ref. [26], MCs were first modified using a standard DA modification procedure known from the literature. Deposition from a 3.3 wt-% DA solution in TRIS buffer over 24 h yielded fairly thick and rough PDA films (12–14 wt% of the capsule mass, mean thickness $\sim$ 300 nm). In ref. [27], DA concentration and modification time were reduced to 1.6 wt-% and 2 h which led to a thinner but still rough layer (2.2 wt-% of the capsule mass, mean thickness $\sim$ 50 nm). The best metallization results on flat surfaces were achieved, however, with very thin PDA films after only 10 min DA modification time [41]. The short reaction time prevented the formation of large agglomerates and created a smooth PDA film suitable for the subsequent metallization.

Therefore, in the present work, as a basis for the metallization of MCs, we used DA modification conditions as in [41]. In contrast to earlier studies where the PDA-coated MCs appeared dark brown [26], the shorter modification time of 10 min led to a light brownish coloration of the initially white capsules (cf. Figure 2a). No change of the optical appearance or reflectivity was observed by confocal microscopy (Fig. 2b). After the metallization step, the MCs appeared black to the bare eye but more shiny in the confocal microscope reflection image. Besides, Fig. 2 b gives an impression of the size distribution and shape of the MCs. Their size ranges from a few

μm up to approx. 30 μm. Not all capsules have a spherical shape; some have collapsed due to unavoidable mechanical pressure applied during storage and transport. However, the degree of deformation does not significantly change after PDA coating and metallization, which proves that the treatment does not cause any evident damage.

Surface morphology

The surface morphology of untreated and modified MCs was studied by SEM (Fig. 3) and AFM (Fig. 4). While the SEM images show selected capsules as a whole, AFM imaging can investigate only small areas (max. 10 μm × 10 μm) in the topmost area of single larger capsules (diameter around 20 μm). Besides the top view of the MCs (Fig. 3a), we also studied cross-cut of the particles by SEM (Fig. 3b). For this purpose, they were embedded in epoxy resin and cut by a diamond knife.

Like the confocal microscopy, the SEM top-view images reveal a broad variety of MC sizes and their non-spherical shape. It is interesting to notice that the neat MCs show a slightly structured surface, which is still visible after the deposition of the thin DA layer. On the other hand, metallization creates a rougher surface. The comparison of the cross-cuts of the embedded MCs (Fig. 3B) proves the formation of a thin, closed Ni film around the capsules, clearly visible thanks to the strong contrast between the metal layer (white/light gray) and matrix (middle gray). The adhesion between capsules and the embedding epoxy matrix seems good because no fissures can be observed.

The surface roughness variation was quantified from the flattened AFM images. Figure 4 presents AFM micrographs of selected MCs showing characteristic features of each capsule type. Three types of images are shown: (A) 10 μm × 10 μm height images, presented as measured; (B) 2 μm x 2 μm height images flattened to remove the spherical shape of the capsules, emphasize the surface structures, and calculate roughness parameters; and (C) 2 μm x 2 μm amplitude error images, representing the first derivative of the height and thus enhancing small structures.

Neat MCs exhibit patchy structures of different sizes leading to a mean roughness Sa $\sim$ 6–13 nm calculated for an area $2 \times 2 \ \mu m^2$. After modification with PDA, the surface becomes smoother. Obviously

Figure 2 **a** Photographs and **b** confocal microscope reflection images of MC powders.
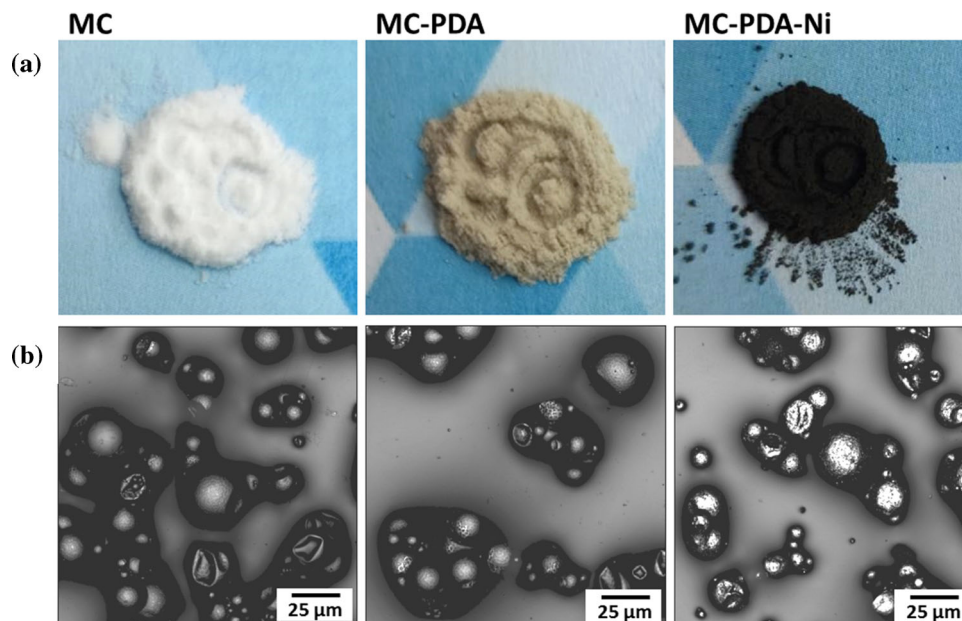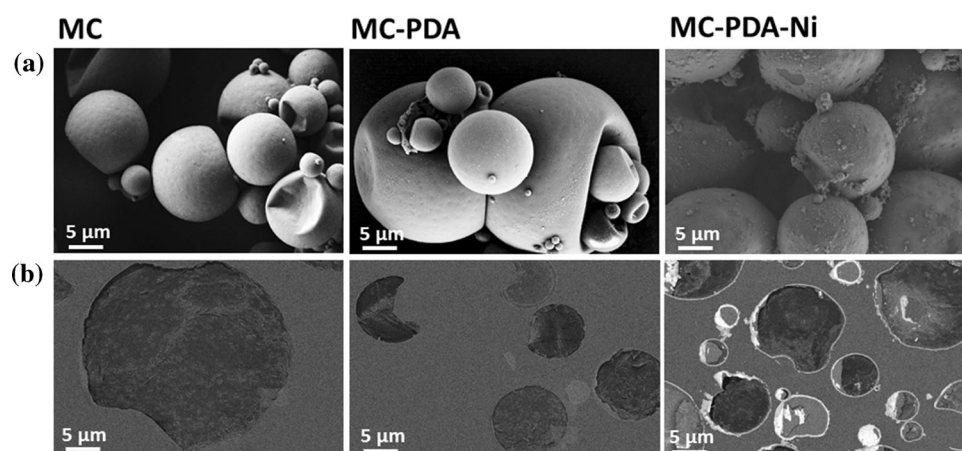

Figure 3 SEM images of MCs: **a** top view; **b** cross-cuts of MCs embedded in epoxy resin.

contaminations on the shell surface are removed during the modification process. In previous work [26, 27], PDA coating over 2 h or 24 h led to PDA layers with roughness of approx. 50 nm and 300 nm, respectively, with a mean surface roughness Sa of up to 86 nm. With the PDA deposition time of 10 min used in this study, the Sa roughness of the PDA-coated MCs is only 3–6 nm. It seems to result not only from the small globular structures of the PDA layer but also from the underlying morphology of the MC shell. On the other hand, after metallization, the roughness increases significantly (Sa $\sim$ 15–30 nm) due to the deposition of flake-like nickel structures.

Spectroscopic investigation

X-ray photoelectron spectroscopy (XPS) is a surface-sensitive technique for qualitative and quantitative elemental analyses of the topmost surface layer (information depth max. 8 nm). Due to its angular dependence, the actual information depth for the MC films was estimated to be less than 4 nm. Figure 5 summarizes high-resolution XPS spectra recorded from neat, PDA-modified and metallized MCs.

The surface region of the neat MC shells essentially consists of the elements carbon, nitrogen and oxygen. From the shape of the C 1 s spectrum (Fig. 5a), it is

Figure 4 AFM images of selected MCs with characteristic surface texture. **a** height images (10 μm × 10 μm); **b** height images (2 μm × 2 μm) after removal of the spherical shape (second-order flattening); **c** amplitude error images (2 μm × 2 μm).
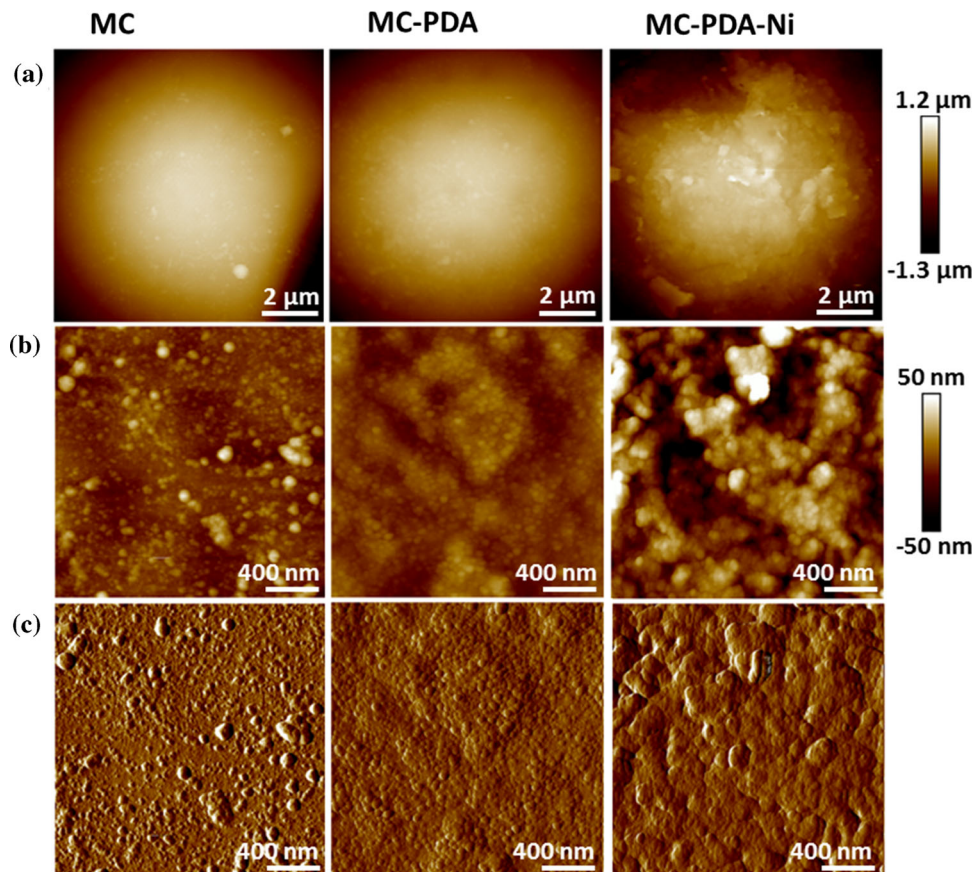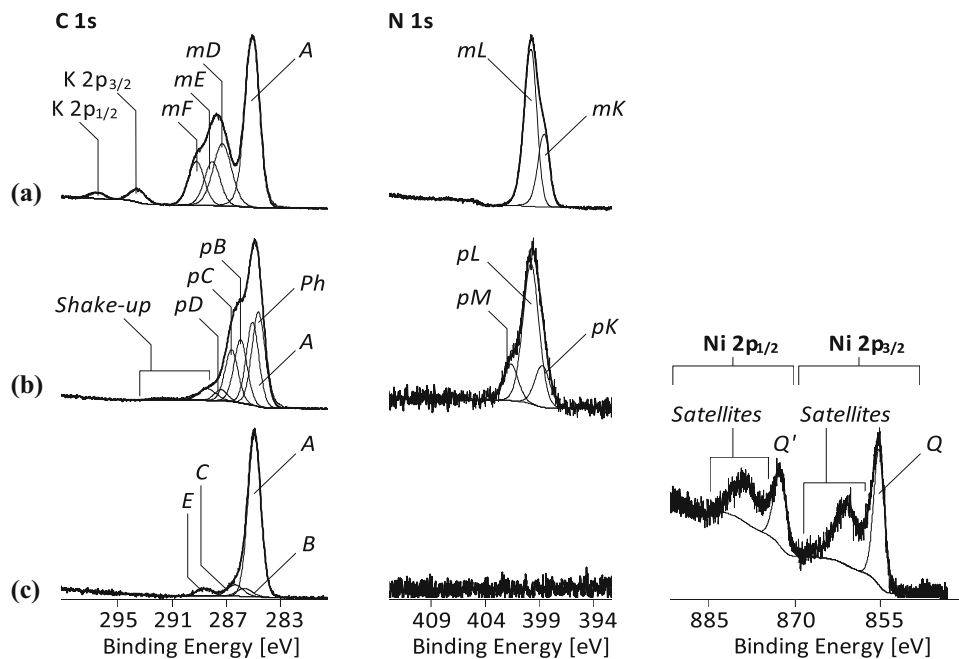

Figure 5 C 1 s (left column), N 1 s (middle column), and Ni 2p (right column) high-resolution XPS spectra recorded from **a** neat MC, **b** MC-PDA, and **c** MC-PDA-Ni.

concluded that the melamine–formaldehyde was cured with urea that condensed the − OH groups of the intermediately formed hexamethylolmelamine.

Figure 5 shows the assignments of the component peaks in the C 1 s and N 1 s spectrum to the corresponding chemical structures given in Fig. 6. The

Figure 6 Presumed chemical structures derived from the C 1 s and N 1 s high-resolution XPS spectra (Fig. 5) of the surfaces of the neat MCs (**a**), PDA-modified MCs (**b**), and the Ni-coated samples (**c**). (**a**) and (**b**) show cut-outs from the polymeric networks; R, R' in (**C**) means alkyl rests. The italic letters indicate the assignment of the carbon or nitrogen atoms to the component peaks of the C 1 s and N 1 s spectra.
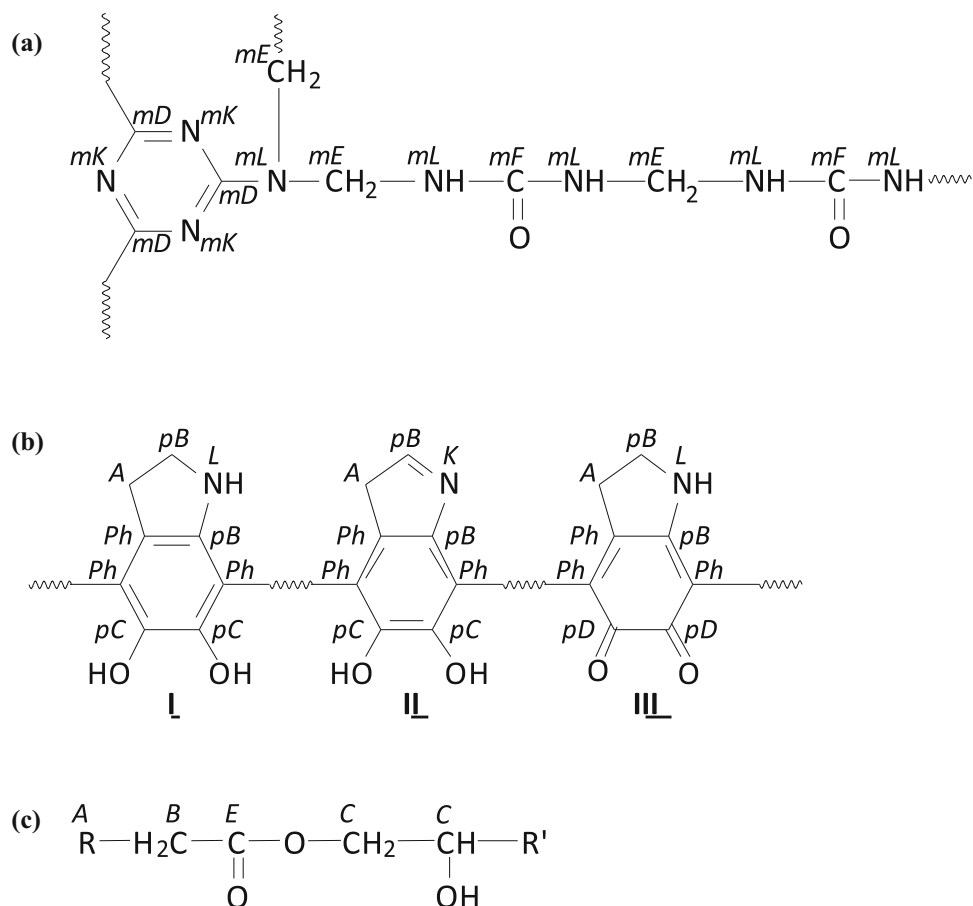
chemical structure of the neat MC surface (Fig. 5a) contains only carbon atoms directly bonded to heteroelements, such as oxygen or nitrogen. Nevertheless, an intense component peak *A* appeared in the C 1 s spectrum at 285.00 eV, indicating the presence of saturated hydrocarbons ($^{A}\underline{C}_xH_y$). In surface analyses, saturated hydrocarbons are usually observed as constituents of surface contaminations when the samples were prepared under ambient conditions or came in contact with the atmosphere. In the MCs, component peak *A* could also result from paraffin having diffused out of the capsules. This would explain the patches on the neat MCs visible in AFM images (Fig. 4). The paraffin coating of the otherwise chemically inert MC surfaces lowers the surface polarity and thus largely prevents acid–base interactions and chemical interactions between the MC surfaces and subsequently applied polymeric matrices.

The deposition of DA on the MC surfaces and its polymerization to PDA changes the shape of the C 1 s and N 1 s peaks significantly indicating that PDA

covers the MC shell completely with a dense polymeric film. At the energy side of the C 1 s spectrum (Fig. 5B), the component peak *Ph* (284.57 eV) evidences the presence of sp²-hybridized carbon atoms of the PDA phenyl rings. Electron transitions between π- and π*-orbitals do not only lead to the dark color observed after the polymerization of DA but also to intensive shake-up peaks at binding energy values higher than 288.2 eV. Carbon–nitrogen bonds ($^{pB}\underline{C}$–N) lead to component peak *pB* at 285.88 eV in the C 1 s spectrum. Its intensity is two-thirds of the intensity of component peak *Ph*. In the corresponding N 1 s spectrum (Fig. 5b), the appearance of a component peak *K* (398.84 eV) on the low-energy side of component peak *L* (399.88 eV) indicates that not only secondary amino groups (^{pB}C–^{pL}$\underline{N}H$–^{pB}C) were formed during the DA polymerization, but also cyclic imides ($^{pB}C = ^{pK}\underline{N}$–$^{pB}C$). The additional component peak *M* at 401.73 eV results from protonated amino groups (^{pB}C–$^{M}\underline{N}^{\oplus}H_2$–$^{pB}C$). Since there are no nitrogen atoms that can be protonated (neither the nitrogen atoms in

the 1,3,5-triazine rings nor the urea nitrogen atoms) in the neat MC polymer, this component peak is absent in the N 1 s spectrum recorded from the neat MCs (Fig. 5a). Component peak pC at 286.53 eV is assigned to the carbon atoms carrying the phenolic OH groups of the PDA's catechol units ($^{pC}\underline{C}$–OH). Its intensity is smaller than that of the component peak pB because some of the DA's phenolic OH groups remain in their quinone-like oxidized state ($^{pD}\underline{C}$ = O; structure $\underline{III}$ in Fig. 5 b). The photoelectrons escaped from the quinone-like bonded carbon atoms are collected as component peak pD at 287.28 eV. The sum of its intensity and the intensity of component peak pC exactly equals the intensity of component peak pB, which agrees with the stoichiometry of PDA (Fig. 5b).

The presence of the Ni 2p peak (Fig. 5c) and the absence of any traces of nitrogen after the metallization proves the formation of a dense and close nickel film on the MCs. Despite this, significant amounts of carbon were detected on the surface of the metallized MC. The shape of the C 1 s spectrum (Figs. 5c) is very characteristic of fats, which usually contaminate surfaces as non-specifically adsorbed substances driven by the high free surface energy of metals and metal oxides [45]. Due to the spin–orbit interaction (spin–orbit effect or spin–orbit coupling) the Ni 2p spectrum is composed of the Ni $2p_{3/2}$ and Ni $2p_{1/2}$ peaks having a coupling constant of ca. 17.4 eV [46]. According to the binding energy of 855.92 eV determined for the main component peaks Q (the corresponding component peaks in the Ni 2p1/2 spectra were designated with Q'), it is assumed that the nickel layer is completely covered by oxidized species, in which nickel is formally present as Ni^{2+} and may exhibit Ni–OH groups. At binding energy values higher than the component peaks Q and Q', the shape of the Ni 2p spectrum appears complex. The intense satellite structures result on one hand from the unpaired electrons in the 3d levels of Ni^{2+} forming a magnetic moment of 2.83 Bohr magnetons, and, on the other hand, from the fact that electronically excited states can also provide photoelectrons after their second photoionization. So no other binding species can be expected in this spectral range.

IR spectroscopy has been used before to characterize PDA layers [42]. Its information depth is, however, in the order of a few micrometers; it lacks sensitivity for thin surface layers. In the case of our very thin PDA film, too, no PDA-specific bands are observable (green curve in Fig. 7a). It is, however, possible to increase the surface sensitivity by optical nearfield enhancement with noble metal clusters localized on the surface (surface-enhanced ATR spectroscopy, SEIRA). For this technique, sub-micrometer-sized silver clusters had to be deposited on top of the PDA layer. For the three-dimensional MCs, this could not be done by physical vapor deposition (PVD) because the silver vapor condenses only on the MC side directed to the silver vapor source. As an alternative, colloidal silver clusters were grown on the MC surfaces by wet chemical metallization. This allows complete, unidirectional cluster coverage of the MCs. The precise adjustment of silver deposition bath parameters enabled the defined cluster growth with the required IR-enhancing properties. The SEM micrographs in Fig. 7b, c highlight the deposited Ag clusters on the MC surface.

The surface-enhanced ATR spectrum of PDA-modified MCs carrying a cluster-like silver layer reveals PDA-specific spectral features in the range of 1200 to 975 cm^{-1} and a band at 455 cm^{-1} (blue curve in Fig. 7a) and thus proves the presence of a thin PDA layer on the MC surface. Studies from previous work [41] have shown that thicker PDA films are not better at mediating adhesion within the interfacial layer – an effect of the granular deposition of the PDA and agglomerated particle formation, which ultimately weakens the mechanical adhesion strength within the interface layers.

Energy-dispersive X-ray spectroscopy (EDX) The elemental composition of broken MC shells was determined by a combination of SEM and EDX at very high magnification. Figure 8 shows an EDX sum spectrum of a Ni-coated MC shell revealing the elements C, N, O, Ni and P.

Figure 9 visualizes the spatial distribution of the elements N, Ni and O. Figures 9a, b show the broken shell at 10,000 × and 100,000 × magnification. In Fig. 9c, d and e, the distribution of N, Ni and O are mapped. For clarity, each element is highlighted in a different color (N – red, Ni – green, O – blue). Superimposing these colored elemental maps with the SEM images (Fig. 9b) gives a clear image of the distribution of selected elements in the MC shell. The inner part is characterized by the presence of nitrogen originating from both melamine–formaldehyde resin and PDA. On the outside, the shell is covered by a thin, closed Ni layer. From SEM and SEM–EDX images, the thickness of the Ni layer was determined to be approx. 50 nm. As postulated from XPS spectra,

Figure 7 a FTIR ATR spectra of the neat MCs (black), the PDA-modified MCs (green) and the surface-enhanced ATR spectrum of PDA-modified MCs covered with Ag clusters (blue); SEM top view **B** and cross-cut **C** images showing the silver clusters deposited on the MS surface.
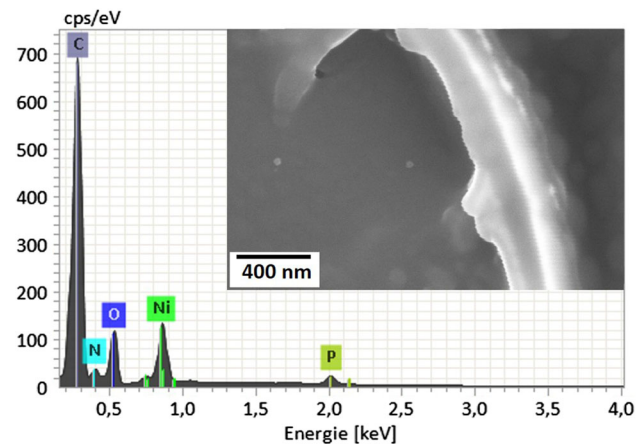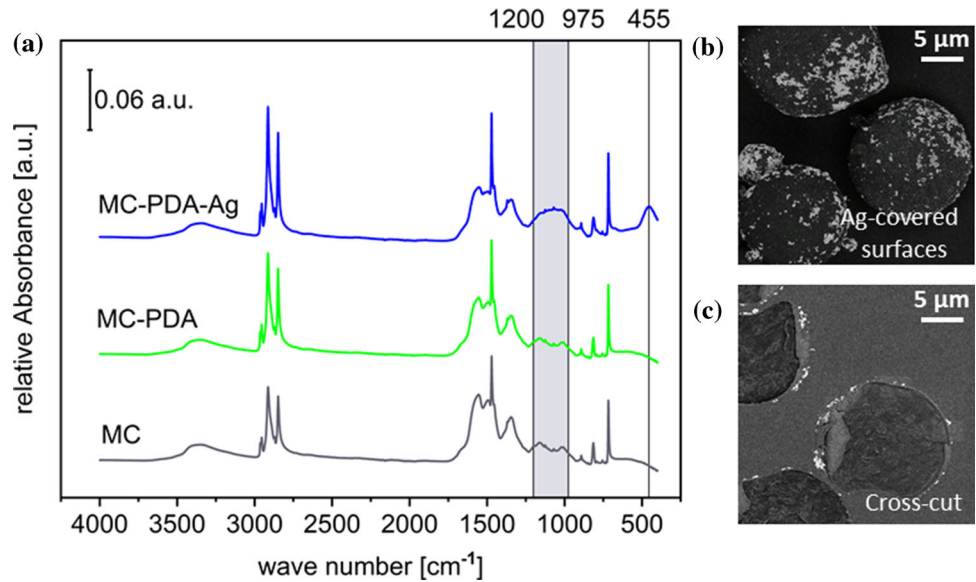
Figure 8 EDX sum spectrum of MC shells covered with Ni.

an oxygen-containing layer can be seen on top of the Ni layer (Fig. 9b, e) – presumably the oxidized Ni surface.

Electrical properties

To study the electrical properties of the metallized MCs, first the macroscopic electrical resistance of the MC powder was measured as a function of the applied mechanical pressure. It was expected that increased pressure leads to higher packing density and an increased contact area between the particles resulting in conductive paths. However, the Ni-coated MCs did not exhibit measurable electrical conductivity up to an applied pressure of 30 MPa. This can be explained by the insulating oxide layer on the nickel coating detected by XPS. Additionally,

deformation or destruction of the capsules may occur under pressure. Then, the capsule core is pressed into the interstices and prevents electrical contact.

To investigate the electrical behavior of the MCs more in depth, the electrical conductivity of single MCs was studied on nanoscopic level by conductive AFM (C-AFM). For this purpose, MCs were attached by conductive silver paste to a conductive substrate. In addition to the sample topography, the electric current between the AFM tip and the substrate was recorded for each point of the MC surface.

Figure 10 shows exemplary AFM topography (amplitude error) and conductivity images of single PDA-modified and metallized MCs. For the non-conducting unmodified and PDA-coated MC, the electrical current was zero in the whole investigated area. With the metallized MCs, however, an electrical current of 10–20 pA was detected when the AFM tip was in contact with the small elevations of the metal layer. This shows that there is a conductive path between these points and the conductive substrate and thus proves the existence of an electrically conductive metal shell of the capsules. The oxide layer detected by EDX and XPS acts, however, as electrical insulation toward the AFM tip. Only at the asperities the cantilever can break through the oxide layer and establish electrical contact.

Overall, the electrical conductivity measurements showed that the most probable reason for the unsatisfactory conductive behavior of the metallized MCs is the oxide layer on top of the deposited Ni film. For applications requiring electrical conductivity of
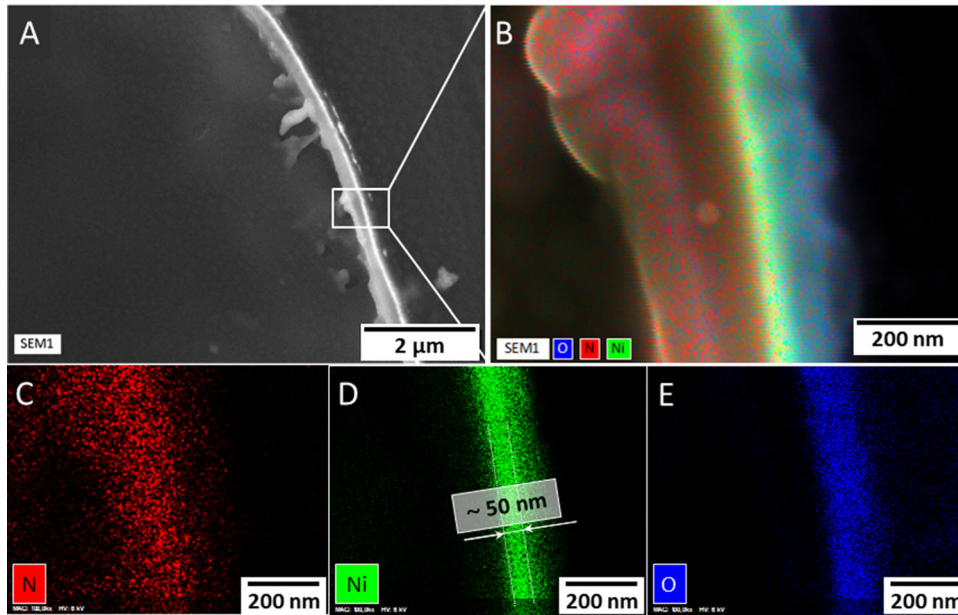
Figure 9 SEM images of the MC shell coated with PDA and Ni: **a** magnification 10,000x; **b** magnification 100,000x; superposition of the SEM image with the corresponding colored elemental maps of N, Ni and O; **c-e** elemental maps of N (**c**), Ni (**d**) and O(**e**) (100,000 × magnification); the elements are highlighted by different colors.
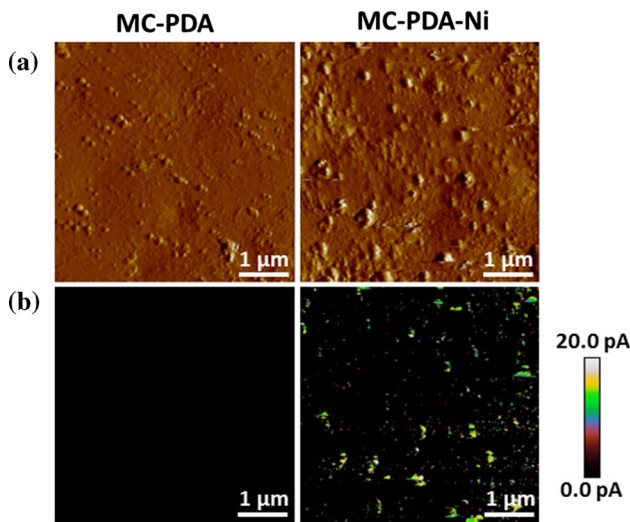

Figure 10 Exemplary C-AFM images of PDA-coated and metallized MCs (image size 5 μm × 5 μm). **a** amplitude error images emphasizing small structures, **b** corresponding images in C-AFM conductive mode.

arrangements of metallized MCs, it is necessary to find a method to suppress the formation of the oxide layer or to remove it. These electrically conductive MC powders could be applied for electro-to-thermal energy conversion and storage, to be heated, e.g., by Joule effect.

Thermal properties

For the application of MCs as thermal storage/management elements, it is of great interest to investigate how metallization affects their thermal properties. Therefore, neat and modified MCs were investigated by thermogravimetric analysis (TGA) and differential scanning calorimetry (DSC), and light flash analysis (LFA). Finally, a test was performed to investigate the possibility of heating the metallized microcapsules via microwave treatment.

Figure 11A shows the TGA thermograms of the neat and coated MCs. As reported in our previous works [26, 27], the thermal degradation of the neat MCs begins with small steps in the temperature interval 100–250 °C, attributable to the degradation of some free (non-encapsulated) paraffin and other low-molecular-weight compounds, residues from the capsule synthesis. Conversely, the degradation event at high temperature, related to the degradation of the capsule core and shell, occurs in a remarkably narrow temperature interval, and the spike in the DTG thermogram suggests a quick and abrupt degradation phenomenon. This spike, also observed in repeated measurements, is less intense for the Ni-coated samples. Additionally, as observed in our previous work on the same MCs coated only with PDA [26], the DTG peak temperature (T_d, see Table 1) of the Ni-
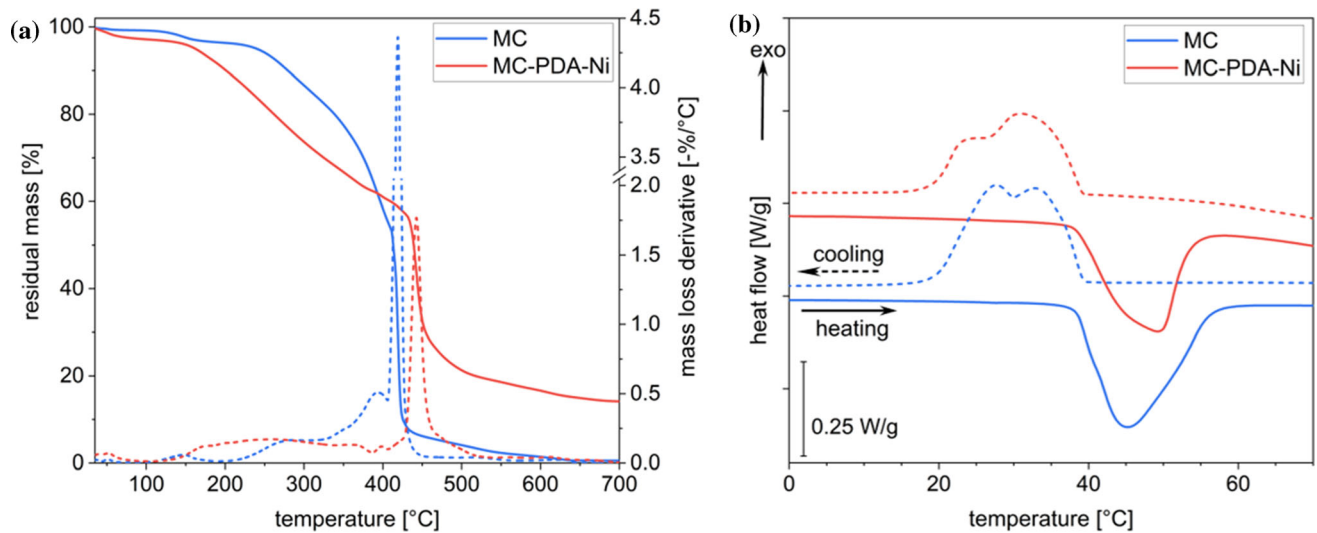
Figure 11 a TGA thermograms of neat and metallized MC. Residual mass (full lines) and mass loss derivative (DTG; dotted lines) as a function of temperature; **b** DSC thermograms of the first heating scan (full lines) and cooling scan (dotted lines) of neat and metallized MC.

Table 1 Main results of the TGA tests of the neat and coated MC

Sample	$T_{1\%}$ (°C)	$T_{3\%}$ (°C)	$T_{5\%}$ (°C)	T_d (°C)	m_r (wt%)
MC	118.4	164.1	241.2	421.2	0.34
MC-PDA-Ni	45.5	111.6	162.1	442.7	14.16

coated capsules is by approx. 20 °C higher than that of neat capsules, which indicates an improvement in the thermal resistance. However, the opposite was observed for the first degradation steps, as for the Ni-coated capsules the values of $T_{1\%}$, $T_{3\%}$, and $T_{5\%}$ are remarkably lower than those of the neat MCs (see Table 1), probably due to the degradation of the PDA coating but also by the release of low-molecular-weight compounds residual from the Ni-coating process. This could partially explain the broad endothermic halo observable for the DSC thermograms of the sample MC-PDA-Ni (see Fig. 11b), starting at the limits of the investigated temperature range (70 °C) in both the first heating and the cooling scans and not anymore observable at the end of the second heating scan (not reported), associable to the irreversible release of low-MW substances. Finally, as expected, the residual mass at the end of the test is by about 14 wt% higher for the coated MCs than for the uncoated ones. The TGA results thus confirm the success of the coating procedure and suggest that the added hybrid coating may be beneficial to mitigate the abrupt thermal degradation of the MCs at high temperatures.

DSC tests were carried out to investigate how the thermal energy storage properties of the microencapsulated PCM have been affected by the metallization. Figure 11B shows the DSC thermograms of the first heating and cooling scans of the neat and coated MC, while the most important DSC results are summarized in Table 2. As found in our previous works on the same PCM [26, 27], the samples show an endothermic signal at approx. 42–45 °C, indicating the melting of the PCM contained in the MC, while the cooling scan shows the corresponding crystallization peak at approx. 30–35 °C. The two local maxima, detectable mainly in the crystallization peak, can be ascribed to the multiple thermal transitions which the PCM undergoes during the phase change, as thoroughly described in our previous works [11, 26, 48, 49]. Since all these transitions contribute to the total phase change enthalpy and are thus responsible for the heat storage/release performance of the PCM, the analysis carried out in this work considers the endo/exothermic peaks as a whole, without further distinctions among the contributions of the single phase transitions.

Table 2 Melting and crystallization temperatures and enthalpies of the neat and metallized MCs obtained by DSC and the relative phase change enthalpy (ΔH_{rel}) calculated using Eq. 1

	MC	MC-PDA-Ni	ΔH_{rel}
Melting temperature (first scan)	42.8 °C	47.2 °C	
Melting enthalpy (first scan)	222.4 J/g	154.6 J/g	69.5%
Crystallization temperature (first scan)	35.4 °C	33.7 °C	
Crystallization enthalpy (first scan)	220.9 J/g	171.8 J/g	77.8%
Melting temperature (second scan)	42.7 °C	46.5 °C	
Melting enthalpy (second scan)	221.7 J/g	156.7 J/g	70.7%

If the coating process does not remarkably modify the transition temperatures, it has a non-negligible effect on the melting and crystallization enthalpy values (Table 2). The phase change enthalpy decreases from 225 J/g of the neat MCs to 150–170 J/g of the metallized sample MC-PDA-Ni. As a first approximation, this decrease has been attributed totally to the mass of the hybrid coating (PDA + metal), which does not contribute to the phase change enthalpy. To quantify this added mass, a relative phase change enthalpy (ΔH_{rel}) has been calculated by normalizing the phase change enthalpy of the coated samples by that of the neat MCs, as shown in Eq. (1):

$$\Delta H_{rel} = \frac{\Delta H(MC - PDA - Ni)}{\Delta H(MC)} \times 100 \qquad (1)$$

This value, which also represents the residual active PCM weight fraction in the coated MCs compared to that of the neat MCs, allows the calculation of the "inactive" mass surplus, i.e., the additional mass in the coated MCs that does not undergo a phase transition. If this mass is attributed totally to the added hybrid coating, the mass of this coating would be the complement to 100 of the relative enthalpy. This added mass is approx. 30 wt% of the sample MC-PDA-Ni—about twice as much as the residual mass obtained by TGA (14 wt%, cf. Table 1). One reason is that the residual mass in TGA comprises only the mass of the solid residues after thermal treatment representing mainly the inorganic Ni coating. To clarify this point, further tests are needed, such as the analysis of the residues after the TGA tests. On the other hand, small fractions of the PCM (likely those having diffused out of the MC shell as suggested by XPS and AFM images) may have been dissolved during the coating procedure which leads to an overestimation of the added mass. In any case, the proposed coating method is proven effective in retaining most of the pristine heat storage/release performance of the uncoated microcapsules. This leads to a much higher melting enthalpy than reported by other authors for silver-coated MCs, e.g., 68 J/g [23], 26–72 J/g [25], and 97 J/g [24].

Finally, the thermal diffusivity of the neat and coated MC powders was evaluated at different temperatures to assess the effect of the hybrid coating on the heat exchange capability of the microencapsulated PCMs (Fig. 12). The results of the PDA-coated MCs are reported for comparison, as they have never been published in our previous works. As expected, for all samples, the diffusivity decreases when the temperature approaches the melting point, as already observed in previous works on polymer composites containing these or similar PCMs [7, 11, 48]. The sole PDA layer causes a decrease in the thermal diffusivity of the powder bed at 25 °C, maybe because of a reduced packing capability of the MCs due to the rougher surface. On the other hand, the nickel layer promotes a remarkable increase in thermal diffusivity. For instance, at 25 °C, the diffusivity of the MC powder bed rises from 0.18 mm²/s of the neat MCs to 0.42 mm²/s of the MC-PDA-Ni sample (+ 130%). These
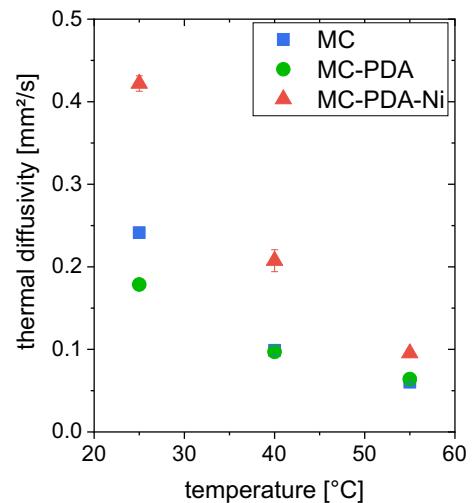

Figure 12 Thermal diffusivity (mean and standard deviation of 5 shots) of the neat and coated MC.

results confirm that a hybrid coating is a good strategy to improve the thermal diffusivity of a PCM powder bed but the coating process must be carefully optimized to enhance the thermal diffusivity without excessively compromising the phase change enthalpy.

A test in a microwave oven was performed to assess the ability of the MCs to be heated by electromagnetic radiation and to act as a thermal management medium. For demonstration purposes, a capsule specimen was prepared by embedding the MCs in a polylactide foil. Figure 13 presents an optical image of this specimen and IR thermograms before (Fig. 13a, b) and after (Fig. 13c) the microwave treatment. This experiment confirmed that the electromagnetic irradiation increased the temperature of the MC-PDA-Ni sample to approx. 40 °C, i.e., the phase change temperature of the PCM.

Further tests were performed to determine the radiation dose to reach a target temperature of 42 °C and the cooling time. Neat, PDA-coated and metallized MCs were treated intermittently in steps of 10 s at 250 W in the microwave oven (2450 MHz) and observed with a thermal imaging camera until the temperature of the MCs reached 42 °C. The results are shown in Fig. 14a. With the metallized MCs, the target temperature could be reached already in two heating steps, i.e., in 20 s while for the plain and PDA-coated MCs a heating time of 70 s was necessary.

To determine the cooling behavior, the samples were heated continuously for 20 s in a microwave oven and placed on a plastic substrate with low thermal conductivity. The temperature decrease was measured vs. time required to reach room temperature (see Fig. 14b). The lower slope of the cooling curve of the metallized MCs shows that they are able to store the thermal energy over a longer time since they also release latent heat during cooling. While the neat MCs cool down from 32 °C to 27 °C in 2 min, the same temperature decrease takes about 6 min for the metallized MCs.

Discussion

In this work, commercial phase change material (PCM) microcapsules (MCs) were metallized with nickel using an ultrathin coating of self-polymerized dopamine (PDA) as an adhesion promoter. This approach was used by several groups to produce silver coatings on PCM MCs with silica [23], PMMA [24] and melamine-resin capsules [25]. They used a standard state-of-the art PDA deposition over 24 h; the metallization procedure resulted in rather rough, particulate silver coatings. While these papers use silver as a metallic phase, our work is focused on the deposition of nickel, which is cheaper and can be deposited as a continuous thin layer. Following on from our previous studies about PDA deposition on PCM MCs [26, 27], a very short PDA deposition time (10 min) was applied to yield an ultrathin adhesive layer as the basis for the subsequent metallization. This short deposition time is a big advantage with regard to industrial application. The polydopamine layer deposited in this work is thinner than most of those reported in the literature, and this leads to less deposited mass and higher residual specific phase change enthalpy after dopamine deposition. The microcapsules presented in this work have a good heat storage/release performance even after polydopamine/nickel deposition, as they retain 70–80% of the initial latent heat, thus reaching 160–170 J/g. This value is significantly higher than reported by other authors for silver-coated microcapsules with a latent heat of 68 J/g [23], 26–72 J/g [25], and 97 J/g [24].

This work for the first time uses surface-enhanced IR spectroscopy (SEIRA) to study ultrathin PDA films. IR spectroscopy has been used before to

Figure 13 Photograph of a PLA foil with embedded MC-PDA-Ni (**a**); IR image (**b**); IR image after microwave stimulation for 20 s (**c**).
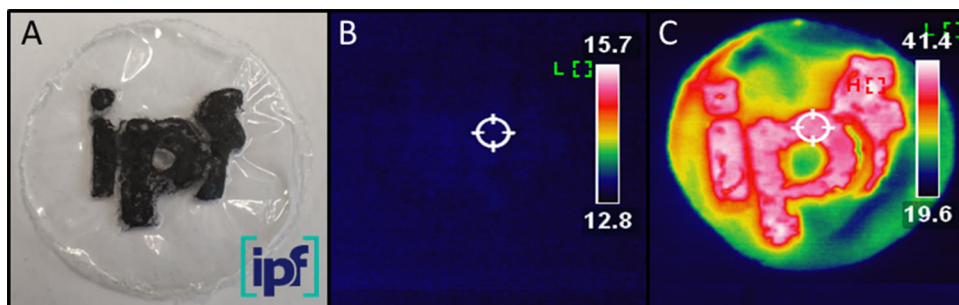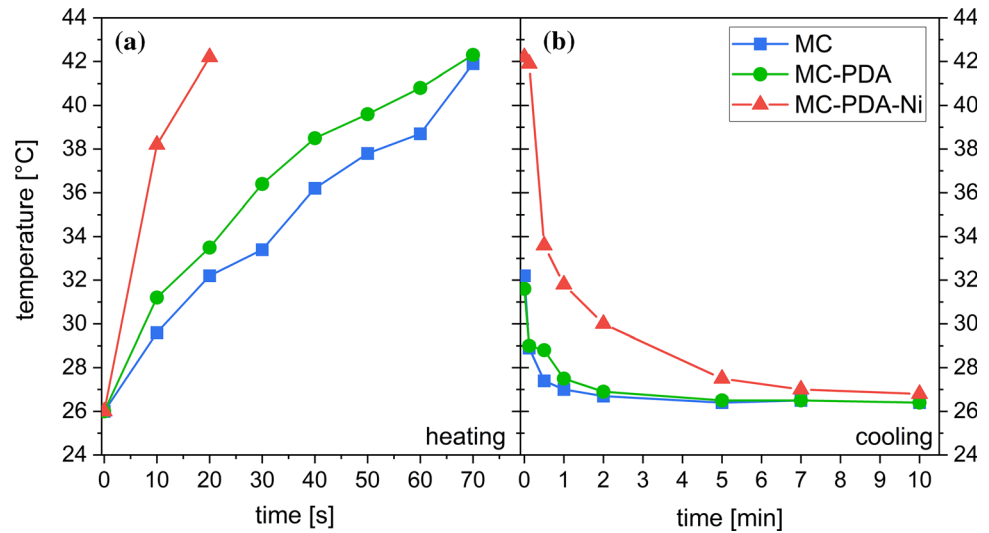
Figure 14 Temperature of plain, PDA-coated and metallized MCs **a** as function of the microwave radiation time (2450 MHz, 250 W), **b** as function of the cooling time after heating for 20 s.

characterize PDA layers [42], showed however, a lack of sensitivity for the ultrathin layer. In SEIRA, high surface sensitivity is obtained by optical nearfield enhancement with silver clusters localized on the surface. In combination with imaging (SEM, AFM) and advanced XPS techniques, the surface chemistry of the coated microcapsules was studied in much more detail than done in earlier studies by other authors. These techniques confirmed the successful PDA deposition by verifying the presence of a thin and well-adherent PDA film onto the MC shells. The PDA layer exhibited small globular structures very similar to the surface features of the neat MCs and did thus not affect the surface morphology. AFM and XPS showed that during PDA deposition, organic contaminations of the shell surface (adsorbed from the environment or diffused from the MC core) were removed.

The metallized MCs were characterized by a broad portfolio of imaging, surface-sensitive spectroscopy, and thermal analysis techniques. AFM, SEM and EDX revealed the creation of a rather rough but compact and continuous Ni layer on the MC. More specifically, the combination of SEM and energy-dispersive X-ray spectroscopy allowed us to spatially resolve the distribution of the elements Ni, N, and O in the MC shell, revealing a Ni layer of approx. 50 nm thickness and a thin, outermost oxide layer. The presence of this oxide layer was the main cause for a non-satisfactory electrical conductivity of the metallized MCs, even though conductive AFM revealed the existence of conductive paths in the Ni layer. Therefore, further studies are needed to prevent the

formation of the oxide layer or to remove it with a post-treatment, in order to produce electrically conductive MC powders that can be applied for electro-to-thermal energy conversion and storage.

Thermal analysis confirmed the success of the coating procedure. TGA results suggest that the added hybrid coating may be beneficial to mitigate the abrupt thermal degradation of the MCs at high temperatures. DSC confirmed the ability of the metallized MCs to undergo phase transition while storing/releasing a large amount of latent heat. The Ni layer had only a minor impact on the melting and crystallization temperature of the PCM core but reduced the melting and crystallization enthalpy due to the extra mass added by the hybrid PDA-Ni coating. This mass is in the order of 20–30 wt-%— comparable to the Ag shell in [24]. Nevertheless, the residual phase change enthalpy is still as high as 170 J/g, which makes the metallized MCs suitable for thermal storage and management applications. The thermal diffusivity of the MC powders was slightly reduced by the PDA film but significantly enhanced by the Ni coating, particularly at room temperature.

It was demonstrated that the PDA/Ni coating makes the PCM microcapsules responsive to electromagnetic stimuli, thereby opening new possibilities for the application of these materials. The application of microwave radiation led to a heating of the MCs from room temperature to the phase change temperature ($\sim$ 40 °C) within 20 s. For plain and PDA-coated MCs, heating over 70 s was necessary to get the same effect. This shows that the contactless transfer and conversion of electromagnetic energy to

heat works very well with the metallized MCs, even with a very thin Ni shell. This is promising for the development of multifunctional and multi-responsive PCM MCs retaining a low gravimetric density and a high phase change enthalpy. Moreover, this heating mechanism does not require contact between the MCs, which suggests the possibility to develop multifunctional polymer composites with an MC concentration below the percolation threshold.

Conclusions

Commercial phase change material (PCM) microcapsules (MCs) were coated with an ultrathin self-polymerized dopamine (PDA) film and subsequently metallized with nickel. A broad portfolio of imaging, surface-sensitive spectroscopy, and thermal analysis techniques was applied for a thorough characterization of the neat, PDA-modified, and metallized MCs.

The thin PDA layer did not alter the surface morphology and roughness of the capsules significantly but could be verified by highly surface-sensitive spectroscopic methods such as XPS and SEIRA. The subsequent metallization step created a rather rough but compact and continuous Ni layer of approx. 50 nm thickness and a thin, outermost oxide layer. This layer limited the electrical conductivity of the MC powder. Thermal analysis revealed that the Ni layer added about 30 wt-% to the MC mass but had only a minor impact on the phase change behavior of the MCs. It enhanced the thermal diffusivity of the MC powders. This makes the metallized MCs suitable for thermal storage and management applications. Finally, microwave irradiation had a stronger heating effect on metallized than on neat or PDA-modified MCs, proving the applicability of the metallized MCs for controlled heating applications.

Overall, this work demonstrates an easy and environmentally friendly technique to produce a thin, uniform, and compact hybrid organic–inorganic coating on PCM microcapsules, which yielded a new multi-responsive and multifunctional material useful for thermal conversion/storage and for thermal management applications. The nature of the bio-based adhesion promotion enables a component separation by decomposing PDA layers. Further studies will be devoted to applying these coated MCs as a multifunctional filler in a polymeric (e.g., epoxy) matrix and to study the interfacial adhesion and the physical–mechanical properties of the resulting composite.

Declarations

References

[1] Pielichowska K, Pielichowski K (2014) Phase change materials for thermal energy storage. Prog Mater Sci 65:67–123. https://doi.org/10.1016/j.pmatsci.2014.03.005

[2] Zhao CY, Zhang GH (2011) Review on microencapsulated phase change materials (MEPCMs): fabrication, characterization and applications. Renew Sustain Energy Rev 15:3813–3832. https://doi.org/10.1016/j.rser.2011.07.019

[3] Chang Z, Wang K, Wu X, Lei G, Wang Q, Liu H, Wang X, Zhang Q (2022) Review on the preparation and performance of paraffin-based phase change microcapsules for heat storage. J Energy Storage 4:103840. https://doi.org/10.1016/j.est.2021.103840

[4] Khadiran T, Hussein MZ, Zaina Z, Rusli R (2015) Encapsulation techniques for organic phase change materials as thermal energy storage medium: a review. Sol Energy Mater Sol Cells 143:78–98. https://doi.org/10.1016/j.solmat.2015.06.039

[5] Lin Y, Zhu C, Fang G (2019) Synthesis and properties of microencapsulated stearic acid/silica composites with graphene oxide for improving thermal conductivity as novel solar thermal storage materials. Sol Energy Mater Sol Cells 189:197–205. https://doi.org/10.1016/j.solmat.2018.10.005

[6] Fredi G, Dorigato A, Pegoretti A (2018) Multifunctional glass fiber/polyamide composites with thermal energy storage/release capability. EXPRESS Polym Lett 12:349–364. https://doi.org/10.3144/expresspolymlett.2018.30

[7] Fredi G, Dorigato A, Unterberger S, Artuso N, Pegoretti A (2019) Discontinuous carbon fiber/polyamide composites with microencapsulated paraffin for thermal energy storage. J Appl Polym Sci 136:47408. https://doi.org/10.1002/app.47408

[8] Fredi G, Dorigato A, Pegoretti A (2019) Novel reactive thermoplastic resin as a matrix for laminates containing phase change microcapsules. Polym Compos 40:3711–3724. https://doi.org/10.1002/pc.25233

[9] Dorigato A, Fredi G, Pegoretti A (2019) Application of the thermal energy storage concept to novel epoxy/short carbon fiber composites. J Appl Polym Sci 136:47434. https://doi.org/10.1002/app.47434

[10] Fredi G, Dorigato A, Fambri L, Pegoretti A (2020) Detailed experimental and theoretical investigation of the thermomechanical properties of epoxy composites containing paraffin microcapsules for thermal management. Polym Eng Sci 60:1202–1220. https://doi.org/10.1002/pen.25374

[11] Fredi G, Dorigato A, Pegoretti A (2020) Dynamic-mechanical response of carbon fiber laminates with a reactive thermoplastic resin containing phase change microcapsules. Mech Time-Depend Mater 24:395–418. https://doi.org/10.1007/s11043-019-09427-y

[12] Cao VD, Pilehvar S, Salas-Bringas C, Szczotok AM, Valentini L, Carmona M, Rodriguez JF, Kjøniksen AL (2018) Influence of microcapsule size and shell polarity on thermal and mechanical properties of thermoregulating geopolymer concrete for passive building applications. Energy Convers Manage 164:198–209. https://doi.org/10.1016/j.enconman.2018.02.076

[13] Singh S, Gaikwad KK, Lee YS (2018) Phase change materials for advanced cooling packaging. Environ Chem Lett 16:845–859. https://doi.org/10.1007/s10311-018-0726-7

[14] Zhu K, Li X, Su J, Li H, Zhao Y, Yuan X (2018) Improvement of anti-icing properties of low surface energy coatings by introducing phase-change microcapsules. Polym Eng Sci 58:973–979. https://doi.org/10.1002/pen.24654

[15] Tomizawa Y, Sasaki K, Kuroda A, Takeda R, Kaito Y (2016) Experimental and numerical study on phase change material (PCM) for thermal management of mobile devices. Appl Therm Eng 98:320–329. https://doi.org/10.1016/j.applthermaleng.2015.12.056

[16] Su W, Darkwa J, Kokogiannakis G (2015) Review of solid–liquid phase change materials and their encapsulation technologies. Renew Sustain Energy Rev 48:373–391. https://doi.org/10.1016/j.rser.2015.04.044

[17] Patchan MW, Baird LM, Rhim YR, LaBarre ED, Maisano AJ, Deacon RM, Xia Z, Benkoski JJ (2012) Liquid-filled metal microcapsules. ACS Appl Mater Interfaces 4:2406–2412. https://doi.org/10.1021/am201861j

[18] Sun D, Zhang H, Zhang X, Yang J (2019) Robust metallic microcapsules: a direct path to new multifunctional materials. ACS Appl Mater Interfaces 11:9621–9628. https://doi.org/10.1021/acsami.9b00827

[19] Tsuneyoshi T, Cui Y, Ishida H, Watanabe T, Ono T (2019) Metal microcapsules prepared via electroless plating at liquid-liquid interface. Langmuir 35:13311–13317. https://doi.org/10.1021/acs.langmuir.9b00181

[20] Olivera S, Muralidhara HB, Venkatesh K, Gopalakrishna K, Vivek CS (2016) Plating on acrylonitrile-butadiene-styrene (ABS) plastic: a review. J Mater Sci 51:3657–3674. https://doi.org/10.1007/s10853-015-9668-7

[21] Cao L, Su D, Tang Y, Fang G, Tang F (2015) Properties evaluation and applications of thermal energystorage materials in buildings. Renew Sustain Energy Rev 48:500–522. https://doi.org/10.1016/j.rser.2015.04.041

[22] Wang W, Jiang J, Wen S, Liu L, Zhang L (2018) Preparation and characterization of polystyrene/Ag core–shell microspheres – a bio-inspired poly (dopamine) approach. J Colloid Interf Sci 368:241–249. https://doi.org/10.1016/j.jcis.2011.10.047

[23] Zhu Y, Liang S, Luo X, Chen K, Tian C, Wang J, Zhang J (2018) Novel metal coated nanoencapsulated phase change materials with high thermal conductivity for thermal energy storage. Sol Energy Mater Sol Cells 176:212–221. https://doi.org/10.1016/j.solmat.2017.12.006

[24] Al-Shannaq R, Kurdi J, Al-Muhtaseb S, Farid M (2016) Innovative method of metal coating of microcapsules containing phase change materials. Sol Energy 129:54–64. https://doi.org/10.1016/j.solener.2016.01.043

[25] Saputro EA, Al-Shannaq R, Farid MM (2019) Performance of metal and non-metal coated phase change materials microcapsules when used in compressed air energy storage system. Appl Therm Eng 157:113715. https://doi.org/10.1016/j.applthermaleng.2019.113715

[26] Fredi G, Simon F, Sychev D, Melnyk I, Janke A, Scheffler C, Zimmerer C (2020) Bioinspired polydopamine coating as an adhesion enhancer between paraffin microcapsules and an epoxy matrix. ACS Omega 5:19639–19653. https://doi.org/10.1021/acsomega.0c02271

[27] Fredi G, Zimmerer C, Scheffler C, Pegoretti A (2020) Polydopamine-coated paraffin microcapsules as a multifunctional filler enhancing thermal and mechanical performance of a flexible epoxy resin. J Compos Sci 4:174. https://doi.org/10.3390/jcs4040174

[28] d'Ischia M, Napolitano A, Ball V, Chen CT, Buehler MJ (2014) Polydopamine and eumelanin: from structure−property relationships to a unified tailoring strategy. Accounts Chem Res 47:3541–3550. https://doi.org/10.1021/ar500273y

[29] Ryu JH, Messersmith PB, Lee H (2018) Polydopamine surface chemistry: a decade of discovery. ACS Appl Mater Interfaces 10:7523–7540. https://doi.org/10.1021/acsami.7b19865

[30] Liebscher J (2019) Chemistry of polydopamine – scope, variation, and limitation. Eur J Org Chem. https://doi.org/10.1002/ejoc.201900445

[31] Ye Q, Zhou F, Liu WM (2011) Bioinspired catecholic chemistry for surface modification. Chem Soc Rev 40:4244–4258. https://doi.org/10.1039/C1CS15026J

[32] Jiang JH, Zhu LP, Zhu LJ, Zhu BK, Xu YY (2011) Surface characteristics of a self-polymerized dopamine coating deposited on hydrophobic polymer films. Langmuir 27:14180–14187. https://doi.org/10.1021/la202877k

[33] Zhou P, Deng Y, Lyu B, Zhang RR, Zhang H, Ma H, Lyu W, YL, Wei SC, (2014) Rapidly-deposited polydopamine coating via high temperature and vigorous stirring: formation. Charact Biofunctional Eval Plus One 9:e113087. https://doi.org/10.1371/journal.pone.0113087

[34] Zimmerer C, Simon F (2016) Metallisierte Oberflächen und Verfahren zu ihrer Herstellung, DE 10 2016 222 943 B3

[35] Zimmerer C (2019) Umweltschonende Verfahrensalternative zur Kunststoffmetallisierung. GAK: Gummi Fasern Kunststoffe 72:198–204.

[36] Zimmerer C, Putzke S, Reinhardt M, Janke A, Stommel M, Hofinger J, Simon F (2021) Bioinspirierte Metallisierung von Polyolefinen. Muschelklebstoff als haftvermittelnde Schicht zwischen Kunststoffsubstrat und Metall. https://www.kunststoffe.de/a/fachartikel/bioinspirierte-metallisierung-von-polyol-324299. Accessed 24 May 2022.

[37] Silva C, Simon F, Friedel P, Pötschke P, Zimmerer C (2019) Elucidating the chemistry behind the reduction of graphene oxide using a green approach with polydopamine. Nanomaterials 9:902. https://doi.org/10.3390/nano9060902

[38] Rezaie AB, Liebscher M, Ranjbarian M, Simon F, Zimmerer C, Drechsler A, Frenzel R, Synytska A, Mechtcherine V (2021) Enhancing the interfacial bonding between PE fibers and cementitious matrices through polydopamine surface modification. Composites B 217:108817. https://doi.org/10.1016/j.compositesb.2021.108817

[39] Bazzaoui M, Martins JI, Bazzaoui EA, Albourine A (2012) Environmentally friendly process for nickel electroplating of ABS. Appl Surf Sci 258:7968–7975. https://doi.org/10.1016/j.apsusc.2012.04.146

[40] Olivera S, Muralidhara HB, Venkatesh K, Gopalakrishna K, Vivek CS (2016) Plating on acrylonitrile-butadiene-styrene (ABS) plastic: Review. J Mater Sci 51:3657–3674. https://doi.org/10.1007/s10853-015-9668-7

[41] Augustine N, Putzke S, Janke A, Simon F, Drechsler A, Zimmerer C (2022) Dopamine-supported metallization of polyolefins - a contribution to transfer to an eco-friendly and efficient technological process. ACS Appl Mater Interfaces 14:5921–5931. https://doi.org/10.1021/acsami.1c19575

[42] Badillo-Ramírez I, Saniger JM, Popp J, Cialla-May D (2021) SERS characterization of dopamine and in situ dopamine polymerization on silver nanoparticles. Phys Chem Chem Phys 23:12158. https://doi.org/10.1039/D1CP00966D

[43] Shirley DA (1972) High-resolution X-ray photoemission spectrum of the valence bands of gold. Phys Rev B 5:4709–4714. https://doi.org/10.1103/PhysRevB.5.4709

[44] Krause B, Boldt R, Häußler L, Pötschke P (2015) Ultralow percolation threshold in polyamide 6.6/MWCNT composites. Composites Sci Technol 114:119–125. https://doi.org/10.1016/j.compscitech.2015.03.014

[45] Zisman WA (1964) In: Gould RF (ed) Contact Angle, Wettability and Adhesion. American Chemical Society, Washington, pp 1–51. doi:

[46] Moulder JF, Stickle WF, Sobol P, Bomben KD, Chastain J (1992) PHI-Handbook of X-ray photoelectron spectroscopy. Perkin-Elmer Corp, Eden Prairie, pp 84–85. doi:

[47] Fredi G, Brünig H, Vogel R, Scheffler C (2019) Melt-spun polypropylene filaments containing paraffin microcapsules for multifunctional hybrid yarns and smart thermoregulating thermoplastic composites. EXPRESS polym lett 13:1071–1087. https://doi.org/10.3144/expresspolymlett.2019.93

[48] Fredi G, Dirè S, Callone E, Ceccato R, Mondadori F, Pegoretti A (2019) Docosane-organosilica microcapsules for

structural composites with thermal energy storage/release capability. Materials 12:1286/1–26. doi: https://doi.org/10.3390/ma12081286

[49] Fredi G, Dorigato A, Fambri L, Pegoretti A (2018) Multifunctional epoxy/carbon fiber laminates for thermal energy storage and release. Composites Sci Techno 158:101–111. https://doi.org/10.1016/j.compscitech.2018.02.005